CrossMark

Hot flow behavior characterization for predicting the titanium alloy TC4 hollow blade surface Sinkage defects in the SPF/DB process

Ning Wang [1] · Minghe Chen [1] · Lansheng Xie [1]

Abstract

Titanium hollow blade is applied in aircraft turbo-machine to gain higher thrust-to-weight ratio. The typical combined super-plastic forming and diffusion bonding (SPF/DB) technology has been widely used in manufacturing complex multi-layer hollow structures such as the titanium hollow blade. This study introduced a TC4 hollow blade with internal reinforcing ribs fabricated with a series of hot forming operations including diffusion bonding, hot twisting, stamping and gas bulging. During the forming process, the blade outer surface will sink at the cavity locations due to lack of internal support. The gas pressure bulging process is necessary to repair the defect and bulge the caved surface to the required profile. In order to predict the TC4 blade deformation during the SPF/DB process, its hot flow behavior in the DB and SPF were separately investigated by carrying out isothermal tensile tests at corresponding temperature range and strain rate range. And taking the initial microstructure influence in consideration, samples which experienced the DB heating history were used to characterize the flow behavior in the SPF processes. A strain hardening form power law equation and a hyperbolic-sine law equation were employed to describe the constitutive relations during the DB and SPF respectively. Both models were calibrated with the hot flow curves and applied in the corresponding forming step finite element (FE) simulations. The blade outer surface profiles extracted from each forming step simulation showed good correlation with the experimental measurement. It proved that the hollow blade surface sinkage defect during the SPF/DB process can be accurately predicted by the FE simulation with the calibrated constitutive models. And the effectiveness of the gas bulging process for repairing the sinkage defect were verified in both simulation and experiment.

Keywords TC4 hollow blade · Superplastic forming and diffusion bonding · Hot flow behavior characterization · Surface defect · Finite element analysis

Introduction

Wide chord fan blade can improve the aerodynamic efficiencies of the aircraft turbofan engines by removing the mid-span damper [1]. Hollow structures with balanced stiffness can contribute to higher thrust-to-weight ratio [2]. The hollow wide chord blade with cavities and complex shape required a unique manufacture process as which is impossible to be manufactured by conventional forming methods like forging, casting and milling [3]. The superplastic forming and diffusion bonding (SPF/DB), typically combined to fabricate

hollow structures with internal reinforcing ribs, have been developed and widely applied in the hollow blade production.

The titanium alloys are essential lightweight materials in aircraft due to the high specific strength and good corrosion resistance [4]. They also exhibited excellent superplasticity and diffusion bondability at elevated temperature. Its SPF/DB feasibility has been investigated by Rockwell International in early 1970s [2] and widely used for forming sandwich structures with internal reinforced cores. Titanium wide cord hollow blade is a representative application which effectively reduced the turbine engine weight and improved the fuel economy as well as the thrust capability [5].

In this study, the $\alpha + \beta$ titanium alloy TC4 was applied for manufacturing a wide cord hollow blade as given by Fig. 1. The blade SPF/DB process is based on the method given by Bichon et al. [6] as illustrated in Fig. 2. In the DB process, the two blade halves with flat inner side and grooves given by Fig. 2a are assembled in the DB tools as Fig. 2b. After heating to the DB

✉ Ning Wang
  meewn1987@nuaa.edu.cn

1   College of Mechanical and Electrical Engineering, Nanjing
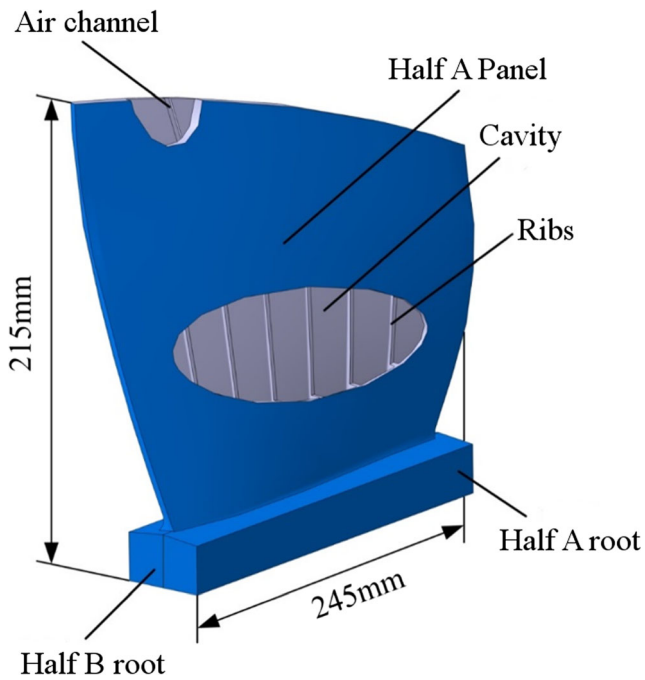   University of Aeronautics and Astronautics, Nanjing 210016, China

Fig. 1 TC4 SPF/DB wide cord hollow blade geometry model

Table 1 As received mechanical properties of TC4 at room temperature

Ultimate Tensile Strength	1321 MPa
Tensile Yield Strength (0.2% offset)	1140 MPa
Uniform Elongation	13.0%
Total Elongation	15.5%

temperature in a vacuum furnace, pressure is applied to the middle flat surface by a hydraulic load cell to weld the specific areas including the reinforcing ribs. At the superplastic temperature and strain rate range, the bonded blade is twisted by the up-end moment meanwhile the blade root is fixed as shown in Fig. 2c. A blade with rough shape can be obtained then. Thereafter, hot stamping and gas bulging are performed in the same tools as shown in Fig. 2d. Continuous gas pressure is loaded in the blade cavity to assure the contact between the blade outer surface and the mold internal surface in the closed tools [1]. In addition, it is necessary to remove the machining allowance by numerical control milling to meet the precision requirement [3].

The TC4 exhibits great temperature and strain rate dependence and its flow stress will drop while the ductility will increase at elevated temperature. In the SPF/DB process, the

blade is heated to high temperature to obtain good bondability and superplasticity. However, due to the low flow stress and the greatly increased formability, the blade surface of the cavity portion where lacks internal support is easily caved under the gravity, the tool restriction on expansion and the torque load. The gas bulging process with sufficient gas pressure and loading time can effectively repair the concave surface. To estimate the forming defects and verify the gas pressure load curve, the numerical finite element analysis (FEA) is very necessary which has showed great capability in metal forming simulation. And a three-dimensional FE simulation work on the titanium hollow blade SPF/DB process has been carried out by Bing et al. [7]. It investigated the influences of the forming rate, friction coefficient and other factors on the forming force and verified the feasibility of the FE method for simulating the hollow blade SPF process. However, as the blade structure and forming process are very different, it is essential to characterize the TC4 flow behavior and establish a unique FE model to predict the two-piece hollow blade deformation during the SPF/DB process.

As the FE simulation accuracy relies much on the material model, it is important to provide a precise constitutive description by performing tensile or compression tests. Investigations on the TC4 hot flow behavior and constitutive modelling have been presented in many published literatures. Sun et al. [8] investigated the TC4 flow behavior in the temperature range from 650 °C to 950 °C which covered the SPF/DB temperature range. At a higher temperature range, Momeni and Abbasi [9] studied the flow behavior in single phase β and dual phase $\alpha + \beta$ regions and a kinetic equation employing the
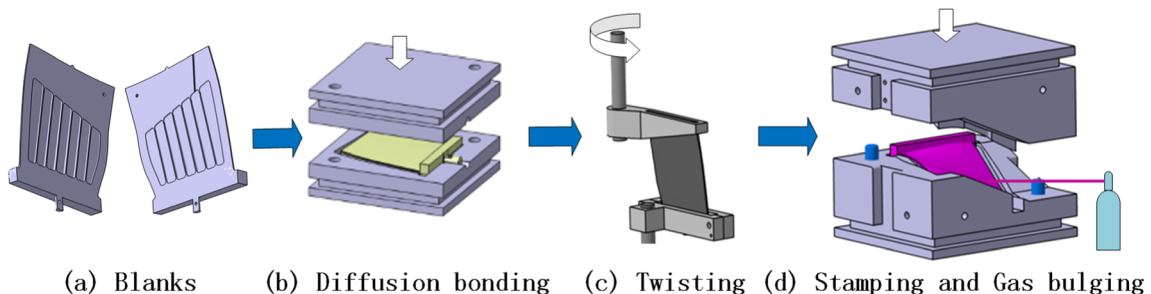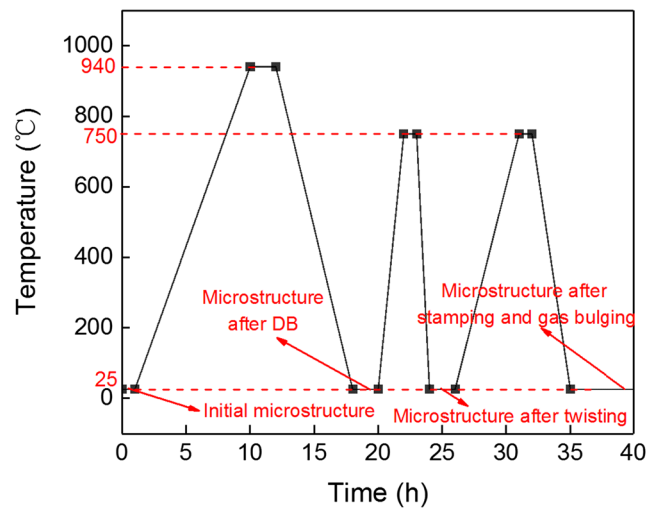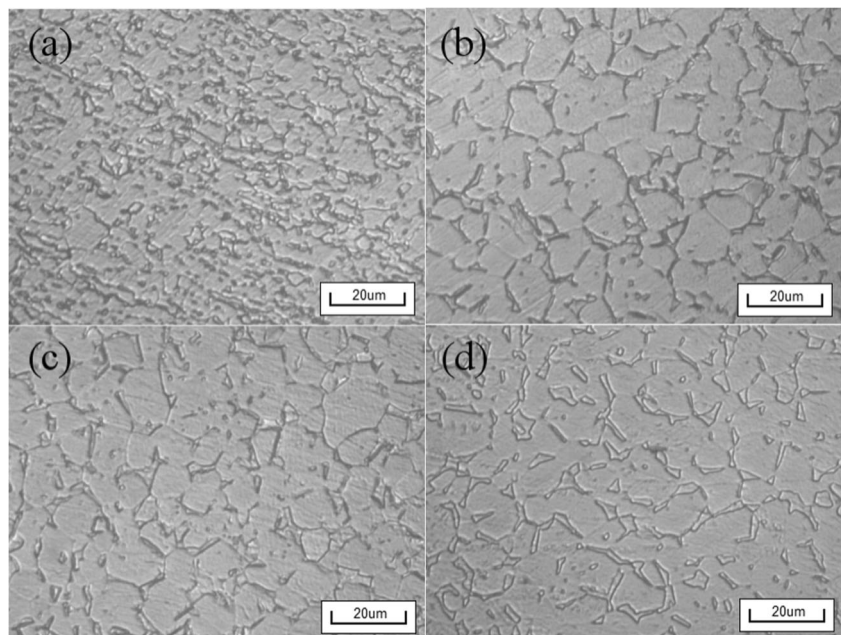

Fig. 2 TC4 SPF/DB wide cord hollow blade manufacturing process

Zenner-Hollomon parameter was applied to describe the peak flow stress at different strain rates and temperatures. Shafaat et al. [10] provided a flow curve model combining the Cingara model and Johnso-Mehl-Avrami-Kolmogorov (JMAK) theory. Bai et al. [11] used a set of mechanism-based constitutive equations to model the softening mechanism in temperature range of 820–1020 °C. In the two-phase temperature range, Zhang et al. [12] studied the superplastic forming behavior of fine-grain size TC4 at 700–850 °C. Quan et al. [13] also studied the TC4 flow behavior and proposed a model for the dynamic recrystallization (DRX). The phase transformation and DRX in isothermal compression tests were simulated by a multi-scale FEM method [14]. Tao et al. [15] employed a modified Arrhenius and artificial neural networks (ANN) models to model the TC4 tube hot compression flow behavior. At lower SPF temperature range, Velay et al. [16] built the constitutive equations to model the viscosity, strain hardening and grain size evolution. However, none of the above researches considered the initial microstructure influences on the hot flow response. In a TC4 isothermal compression study performed by Luo et al. [17], the effect of the alpha grain size on the flow behavior was investigated. It verified that the flow stress increased with larger equiaxed alpha phase volume fraction and the flow stress decreased with increased alpha phase grain size. As the TC4 hollow blade is first diffusion bonded at a temperature over 900 °C leading to phase transformation and grain growth, the microstructure evolution is very necessary to be taken into consideration for characterizing the follow-up SPF flow behavior.

In the FE simulation work carried out by Bing et al. [7], a Backofen equation ignoring the temperature and strain effects

Fig. 4 Heating paths for the SPF/DB forming process microstructure evolution investigation

on stress was employed in the FE model and the forming defects of the blade cavity portion was not predicted. Though Wu et al. [18, 19] has predicted the blade outer surface groove during twisting using a creep model at 750 °C, the blade deformation during diffusion bonding process was not simulated and the temperature effect was neglected. And yet no simulations have taken the diffusion bonding heating history effects on the TC4 flow behavior into consideration. Aiming at predicting and repairing the TC4 hollow blade surface sinkage defects during DB/SPF forming process, this study characterized the TC4 hot flow behavior and simulated the hollow blade deformation in each forming step based on

Fig. 3 TC4 microstructure evolution during SPF/DB process: **a** initial microstructure; **b** microstructure after DB heating path; **c** microstructure after DB and hot twisting heating path; **d** microstructure after DB, hot twisting, stamping and gas bulging heating path

Table 2 Measurements of the primary alpha volume fraction and size at each step

Forming Step	Initial	DB	Twisting	Stamping and gas bulging
Volume fraction (%)	71.09	82.67	84.83	87.21
Diameter-mean (μm)	10.57	12.25	12.69	13.92
Size-length (μm)	14.84	17.09	16.87	17.00
Size-width (μm)	8.17	9.09	9.27	10.05

the experimental works carried out by Wu et al. [18, 19]. The TC4 flow behavior under the DB temperature range and strain rate range was first investigated. And in consideration of the initial microstructure effects, the samples which went through the DB heating path were used for characterizing the flow behavior during the SPF process. Creep models implanted in the commercial FEA software Abaqus were employed for constitutive modelling and applied in the hollow blade SPF/DB FE simulation. The FE model accuracy were evaluated by comparing the outer surface profiles of the simulation results with the experimental measurements.

Experiments

As-received material properties

The as-received TC4 for carrying out the hot tensile tests is 1.0 mm thick hot rolled plate with the composition of 5.5–6.8 wt.% Al, 3.5–4.5 wt.% V, 0.3 wt.% Fe, 0.1 wt.% C,
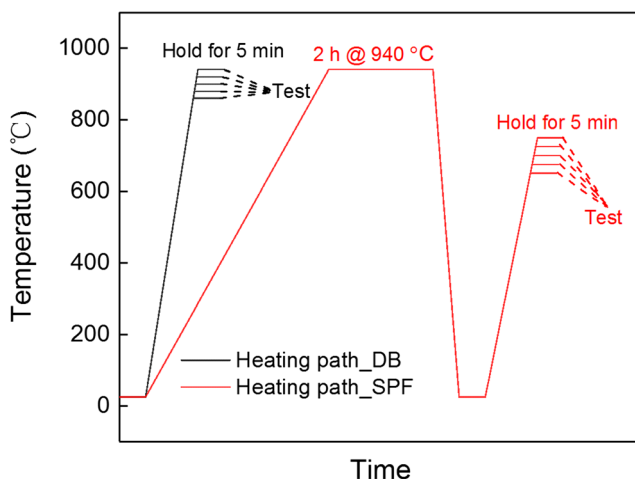
Fig. 5 Heating paths for hot tensile tests

0.05 wt.% N, 0.0115 wt.% H and 0.2 wt.% O. The room temperature mechanical properties are given in Table 1.

Microstructure evolution in SPF/DB processes

The as-received TC4 microstructure is given in Fig. 3a. The heating paths in Fig. 4 were applied to study the SPF/DB heating history effects on the microstructure evolution. The strain path effects on the recrystallization kinetics and grain size could sufficiently lead to significant errors for the flow behavior prediction [20]. In this study, the simulation results of the blade forming processes showed that the maximum equivalent creep strains of the DB, twisting, stamping and gas bulging were 0.08425, 0.08008, 0.6331 and 0.0007957 respectively. As the deformation was relatively small in the DB and twisting process and the stamping and gas bulging were regarded as a continuous process, the deformation influences on the microstructure evolution and flow behavior were not discussed in this paper. And this may be the major simulation error factor for the blade surface sinkage prediction. The distortion of the yield surface associated with the tension–compression asymmetry was observed for a TA6V alloy [21] which indicated that the strain path can make strong impacts on the flow behavior. And in the SPF/DB forming process, the blade experienced deformations including tension, compression and torsion. But due to the relatively small deformation in the DB and twisting process as mentioned above, the tension/compression asymmetry was not considered. And this also could be a critical source of prediction error.

Figure 3b gives the microstructure after 2 h stay at 940 °C in a vacuum furnace which simulated the DB heat treatment. The alpha phase shows obvious increase in grain size and volume fraction. In the SPF twisting process, the TC4 was heated to 750 °C and hold for 1 h. The corresponding microstructure after twisting is shown in Fig. 3c which exhibits a microstructuredynamic recrystallization similar to that before twisting. And Fig. 3d is the microstructure after the representative heat treatment of the gas bulging process during which the TC4 was heated to 750 °C and hold for 1 h. The volume fraction and averaged size of primary alpha of a 171.43 μm × 128.57 μm area at each step were measured by the image analysis program Image-Pro Plus. as given in Table 2.

Experimental procedures

Figure 3 shows that the alpha phase volume fraction and grain size grain size significantly increased in the DB process while the SPF twisting heating history made minor influence on the microstructure evolution. Considering the initial microstructure influence, the samples used to characterize the flow

Table 3 Experimental matrix of TC4 hot uniaxial tensile test

	DB Tensile tests	SPF Tensile tests
Orientation	Longitudinal	Longitudinal
Strain Rate (s^{-1})	0.0001,0.0003,0.0005,0.0007	0.001,0.01, 0.1
Temperature (°C)	860, 880, 900, 920, 940	650, 675, 700, 725, 750

behavior during SPF twisting, stamping and gas bulging were first heated to the DB temperature 940 °C and hold for 2 h in a vacuum furnace. The heating paths for the tensile tests at the DB and SPF temperatures are illustrated in Fig. 5.

The experiment matrix for TC4 isothermal uniaxial tensile tests are given in Table 3. The temperatures and strain rates were determined according to previous FE simulation results of the hollow blade SPF/DB process [18, 19]. In the DB tensile tests, both the temperature range and strain rate range are much narrower than the SPF tensile tests because the DB occurs in a strict temperature range at very low deformation rate.

The tensile sample geometry was designed according to the ASTM E2448 as shown in Fig. 6c. And the fixture is given in Fig. 6b. The isothermal tensile tests were carried out on a SUNS UTM5000 electronic universal testing machine equipped with an environment chamber. In the tensile test, the tensile sample was mounted in the tensile grips, heated to the target temperature and hold for 5 min and then tested at the targets strain rate.

Experiment results

One true stress-true strain curve is plotted for each combination of temperature and strain rate as given by Figs. 7 and 8. Figure 7 summarizes the flow curves at the DB

strain rate range of the 1×10^{-4} s^{-1} to 7×10^{-4} s^{-1} and temperature range of 860–940 °C. At the all strain rates tested of the temperatures above 900 °C and the relative low strain rates of 860 °C and 880 °C, a unique steady hardening behavior can be observed which is very different from the typical dynamic recrystallization and recovery. At the strain rate of 7×10^{-4} s^{-1} of both 860 °C and 880 °C, the flow curves show an initial steady region indicating that the dynamic recovery or grain boundary sliding is the dominant deformation mode. The subsequent strain hardening shows that the deformation mechanism changes with increased strain [22]. Figure 8 gives the flow curves at the SPF temperature range of 650–750 °C and strain rate range of 10^{-3}–10^{-1} s^{-1}. Each curve has a single stress peak after initial strain hardening and a subsequent linear decrease till failure. The peak flow stress and softening behavior indicate that the dynamic recrystallization and the dynamic recovery are the dominant deformation mechanism under the SPF temperature and strain rate scope. Meanwhile, the temperature softening effects are obvious in both the DB and SPF tensile tests. The strain rate has minor effects on the flow stress under the DB temperatures compared with the flow curves of SPF temperatures because of the narrow strain rate scope applied in the DB tensile tests. It verifies that the TC4 flow stress is sensitive to the temperature and strain rate.

Fig. 6 Tensile sample and grips: **a** tensile sample; **b** tensile grips; **c** tensile sample geometry (in mm)
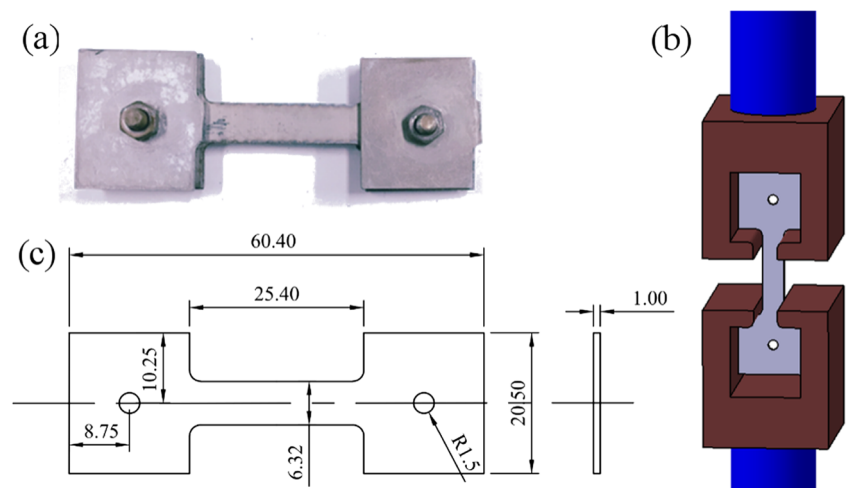
Fig. 7 True stress-true strain curves of TC4 DB tensile tests sorted by temperature

(a) 860 °C

(b) 880 °C

(c) 900 °C

(d) 920 °C

(e) 940 °C
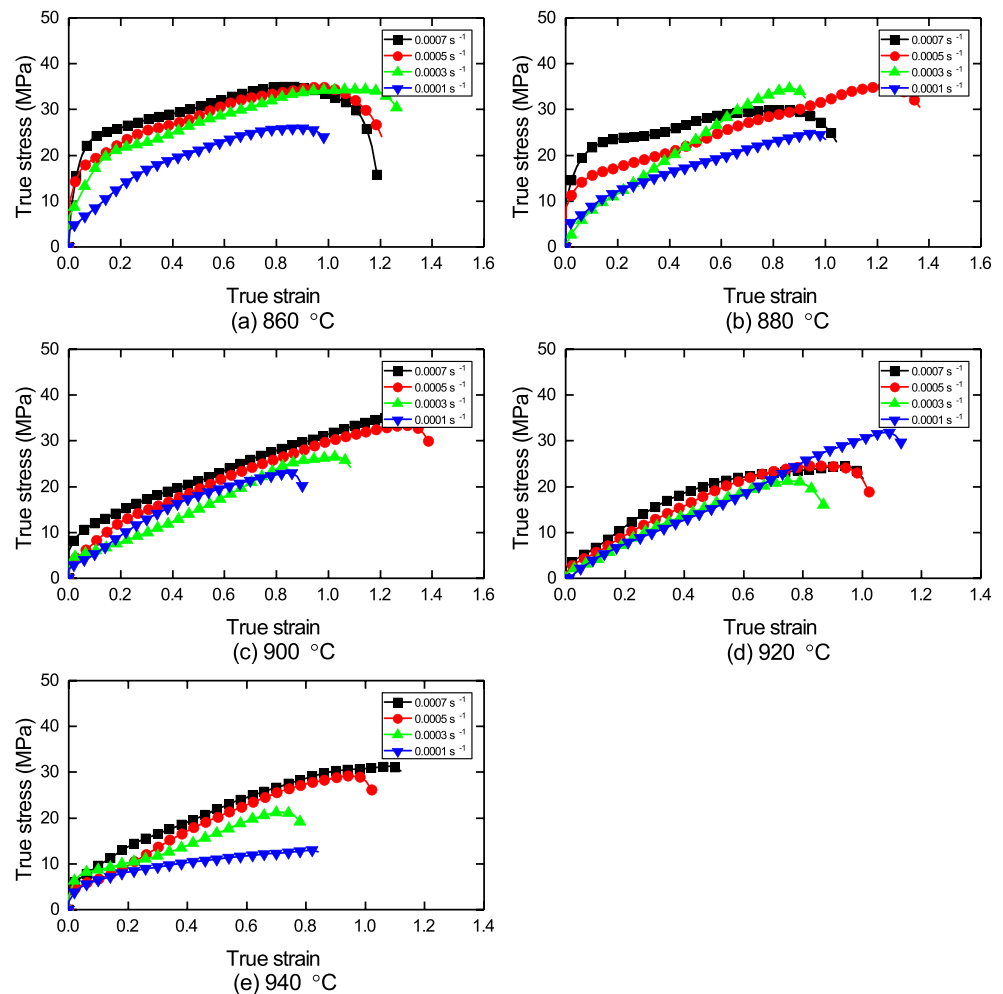
Constitutive modeling

As the TC4 flow curves exhibit strong dependence on temperature and strain rate under the SPF/DB deformation conditions, precise constitutive models capable of describing the temperature and strain rate effects on flow stress are important for the FE modelling. And due to the pronounced hardening behavior shown in Fig. 7, the constitutive model used for DB flow behavior description also needs to take the strain hardening effect into consideration. Although the flow curves show initial strain hardening and subsequent softening in the SPF tensile tests, only the increasing portions can be used for constitutive modelling because a smooth and monotonically increasing stress-strain curve input is required by the FEA software Abaqus (version 6.10) to prevent spurious behavior. Constitutive models in different forms for the creep behavior definition are provided by Abaqus. The strain hardening form creep model expresses the creep strain rate as a function of strain and stress. And the equation coefficients can be input as

temperature dependent which make it qualified for modeling the DB stress-strain curves. For the TC4 constitutive modelling at the SPF temperatures, the peak stress points were applied to calibrate the hyperbolic-sine law model which ignores the strain effects on stress.

A strain hardening form power law equation for DB creep behavior modelling

The strain hardening form power law equation for modelling the creep deformation during DB was given by Eq. (1):

$$\dot{\bar{\varepsilon}}_C = \left\{ A\bar{\sigma}^n \left[(m+1)\bar{\varepsilon}_C \right]^m \right\}^{m+1} \tag{1}$$

where $\dot{\bar{\varepsilon}}_C$ is the uniaxial equivalent creep strain rate in s^{-1}, $\bar{\sigma}$ is the uniaxial equivalent deviatoric stress in MPa which equals 2/3 of the uniaxial stress, $\bar{\varepsilon}_C$ is the equivalent creep strain, and A, n and m are defined as functions of temperature. A and n must be positive and $-1 < m \leq 0$.

Fig. 8 True stress-true strain curves of TC4 SPF tensile tests sorted by temperature

(a) 650 °C

(b) 675 °C

(c) 700 °C

(d) 725 °C

(e) 750 °C
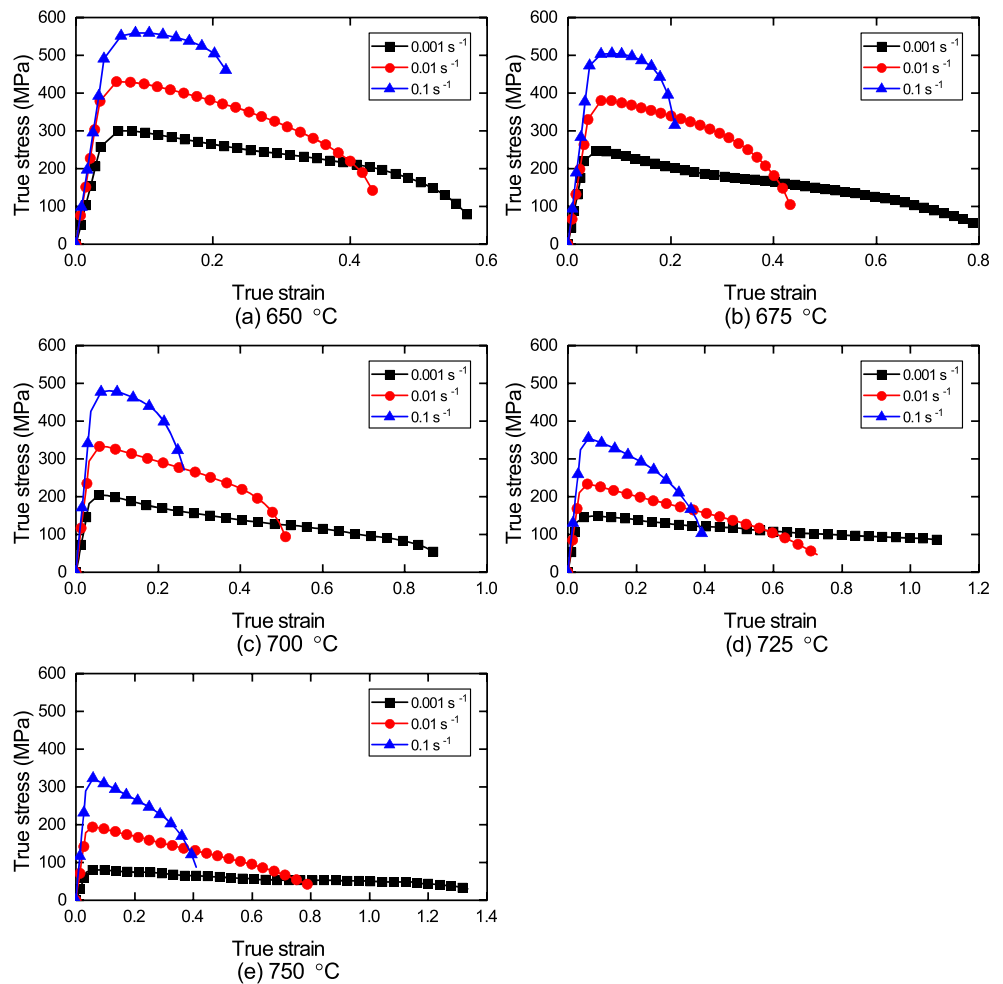
Taking the natural logarithm of both sides, a relation can be obtained as following:

$$ln\left(\overline{\sigma}\right) = -m/n*ln\left(\overline{\varepsilon}_C\right)$$
$$+ (m+1)/n*ln\left(\dot{\overline{\varepsilon}}_C\right) - ln(A)/n - m/n*ln(m+1) \tag{2}$$

Taking $ln(\overline{\varepsilon}_C)$ and $ln(\dot{\overline{\varepsilon}}_C)$ as the independent variables and $ln(\overline{\sigma})$ as the dependent variable, the data points of $ln(\overline{\sigma})$ -$ln(\overline{\varepsilon}_C)$, $ln(\dot{\overline{\varepsilon}}_C)$ were applied in the surface fitting for Eq. (2) by the nonlinear least squares fitting method as shown in Fig. 9. The calibrated coefficients for different temperatures are given in Table 4. The m values are close to -1 which indicates that the calibrated model has minor strain rate dependence.

To evaluate the model prediction accuracy, the mean square error (MSE) and correlation coefficient R were calculated by Eqs. (3) and (4):

$$MSE = \frac{1}{n}\sum_{i=1}^{n}\left(\hat{\overline{\sigma}}_i - \overline{\sigma}_i\right)^2 \tag{3}$$

$$R = \frac{\sum_{i=1}^{n}\left(\overline{\sigma}_i - \overline{\overline{\sigma}}\right)\left(\hat{\overline{\sigma}}_i - \overline{\hat{\overline{\sigma}}}\right)}{\sqrt{\sum_{i=1}^{n}\left(\overline{\sigma}_i - \overline{\overline{\sigma}}\right)^2 \sum_{i=1}^{n}\left(\hat{\overline{\sigma}}_i - \overline{\hat{\overline{\sigma}}}\right)^2}} \tag{4}$$

where n is the number of picked data points on the equivalent deviatoric stress vs. equivalent creep strain curves, $\overline{\sigma}$ and $\hat{\overline{\sigma}}$ are the experimental and calculated equivalent deviatoric stress in MPa, $\overline{\overline{\sigma}}$ and $\overline{\hat{\overline{\sigma}}}$ are the mean experimental and calculated equivalent deviatoric stress in MPa.

The correlations between the calculated equivalent deviatoric stress and the experimental results at different temperatures are shown in Fig. 10. And the MSEs at each combination of temperature and strain rate are plotted in Fig. 11. Both R values and MSEs show that the calibrated creep model gives better prediction for the constitutive relations at 900 °C and 920 °C. It is because that this calibrated strain hardening form power law model has little strain rate dependence and the flow curves at both 900 °C and 920 °C are close to each other showing minor strain rate effects.
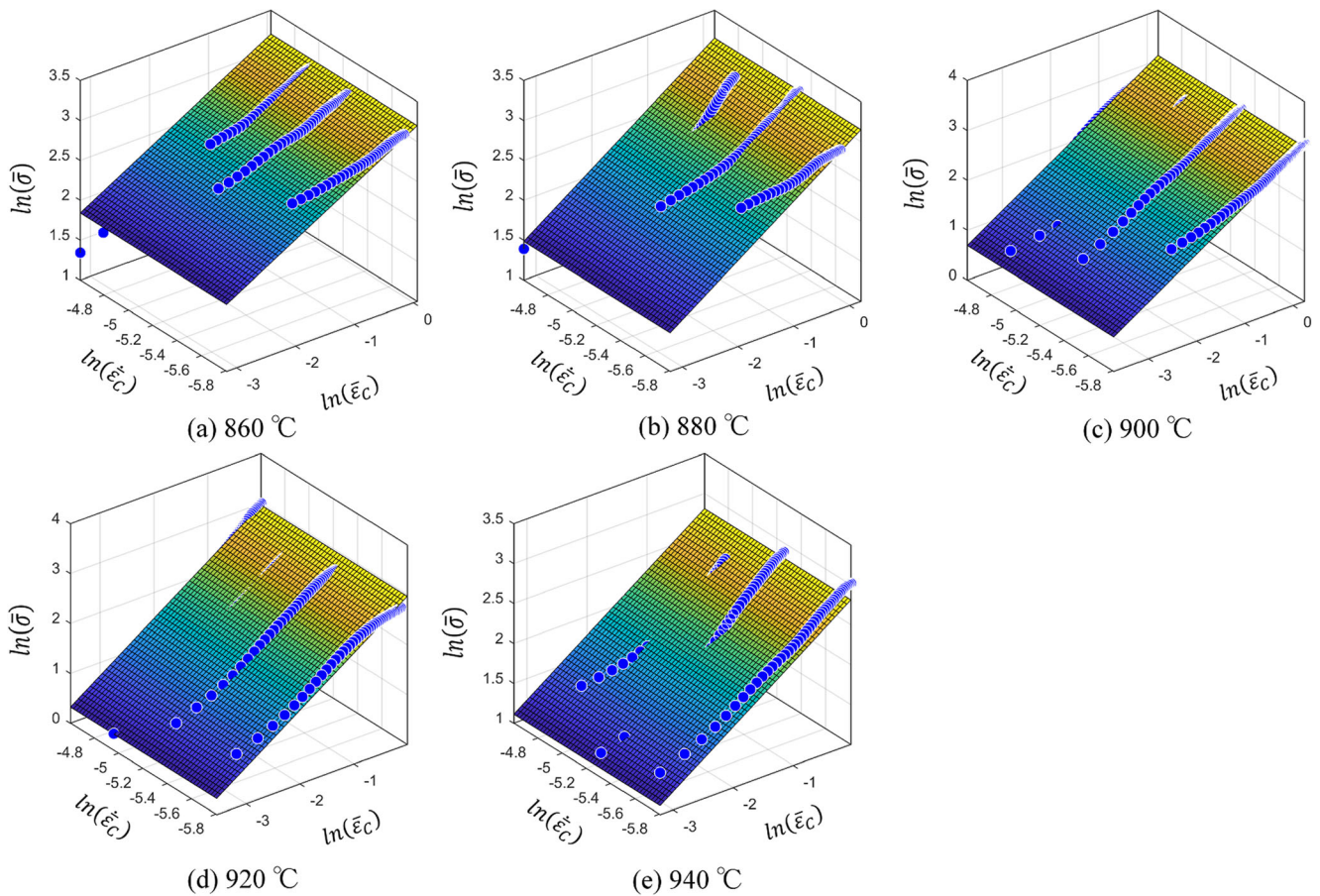
Fig. 9 Calibration of the strain hardening form power law equation with $ln(\overline{\sigma})$ -$ln(\overline{\overline{\varepsilon}}_C)$, $ln(\dot{\overline{\varepsilon}}_C)$

A hyperbolic-sine law equation for SPF creep behavior modelling

The hyperbolic-sine law equation for modelling the creep deformation was given by Eq. (5)

$$\dot{\overline{\varepsilon}}_C = A\left[sinh\left(B\overline{\sigma}\right)\right]^n exp\left(-\frac{Q}{RT^*}\right) \quad (5)$$

where $\dot{\overline{\varepsilon}}_C$ and $\overline{\sigma}$ are as mentioned above, Q is the activation energy in J/mol, R is the universal gas constant 8.314 J/(mol*K), $T^* = (T - T_0)$, T is the temperature in K, T_0 is the temperature of absolute zero 0 K, A, B and n are material parameters. And this equation can be expressed as following:

$$\overline{\sigma} = \frac{1}{B}ln\left\{ \left[\frac{\dot{\overline{\varepsilon}}_C}{Aexp\left(-\frac{Q}{RT^*}\right)}\right]^{\frac{1}{n}} + \left\{1 + \left[\frac{\dot{\overline{\varepsilon}}_C}{Aexp\left(-\frac{Q}{RT^*}\right)}\right]^{\frac{2}{n}}\right\}^{0.5} \right\} \quad (6)$$

Taking the peak stress values of each flow curve, Eq. (6) can be fitted with $\dot{\overline{\varepsilon}}_C$ and T^* as the independent variables and $\overline{\sigma}$ as the dependent variable by the nonlinear least squares fitting method. The fitting results is shown in Fig. 12. And the obtained equation coefficients are $A = 7.717E8$ s^{-1}, $B = 0.005454$ MPa^{-1} $Q = 2.131E5$ J/mol and $n = 3.829$.
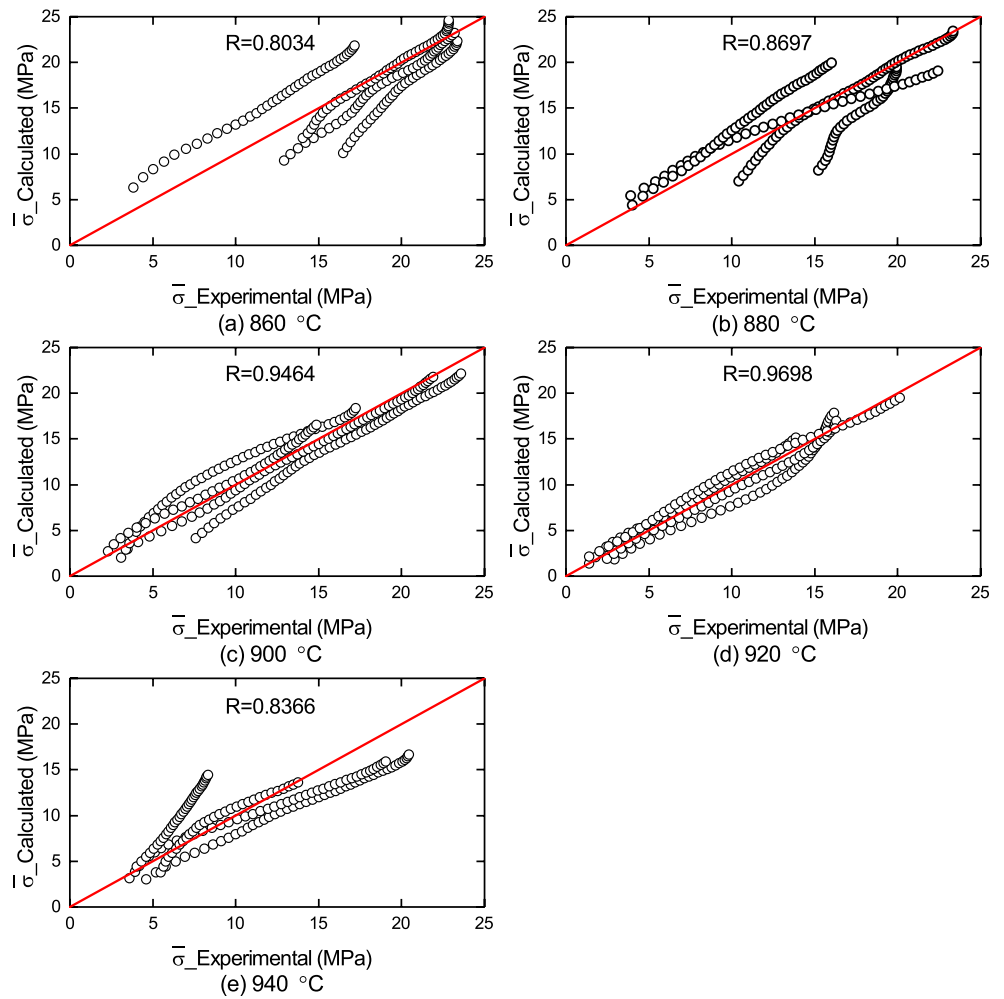
The correlations between the calculated equivalent deviatoric stress and the experimental results at different temperatures are shown in Fig. 13. The total MSE is 561.17. And

| Table 4 Coefficients of the strain hardening form power law equation	Temperature (°C)	860	880	900	920	940
	m	−0.99985	−0.99992	−0.99997	−0.99997	−0.99997
	n	2.37	2.05	1.65	1.34	1.87
	A	7.80E-08	1.43E-07	2.25E-07	5.36E-07	1.55E-07

Fig. 10 Correlations between the calculated equivalent deviatoric stress by the strain hardening form creep model and the experimental results at different temperatures

(a) 860 °C

(b) 880 °C

(c) 900 °C

(d) 920 °C

(e) 940 °C

the MSEs at different temperatures and strain rates are plotted in Fig. 14. It indicates that the hyperbolic-sine law equation

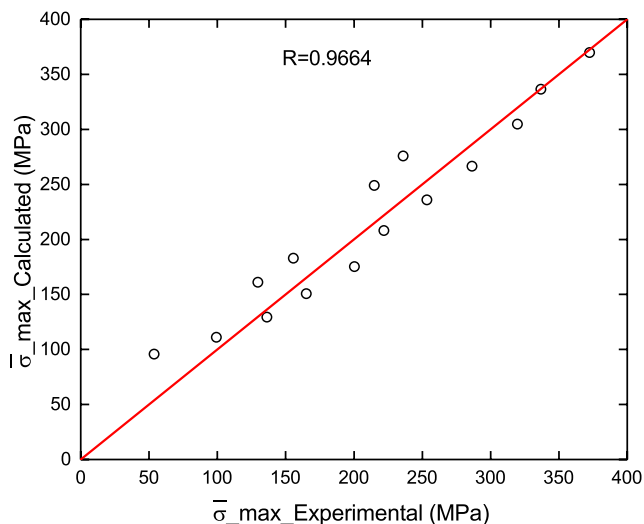can accurately predict the peak flow stress in the SPF temperature and strain rate scope. Better predictions were obtained at
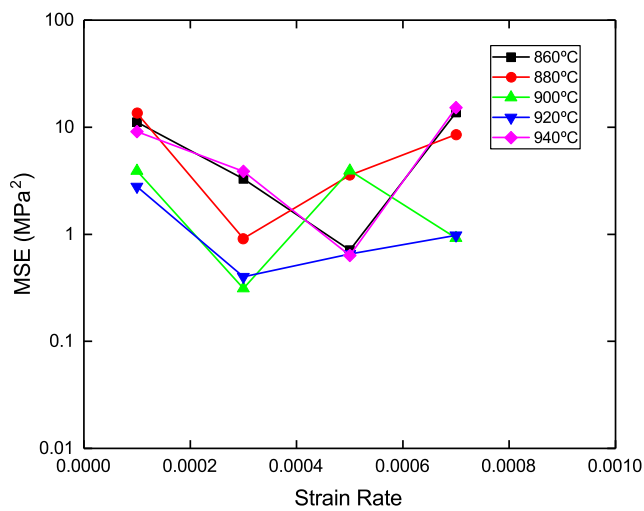
Fig. 11 MSEs of the strain hardening form creep model at different temperatures and strain rates
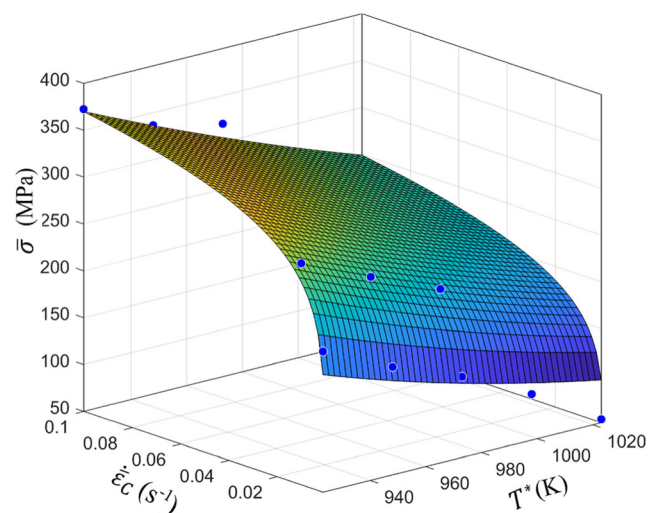
Fig. 12 Calibration of the hyperbolic-sine law equation with $\overline{\sigma}$ -T^*, $\dot{\overline{\varepsilon}}_C$

Fig. 13 Correlations between the calculated max equivalent deviatoric stress by the hyperbolic-sine law model and the experimental results

the temperatures of 675 °C and 700 °C. And it shows little difference in the peak stress prediction accuracy for different strain rates.

Finite element analysis

Based on the TC4 hollow blade SPF/DB process, FE models have been established to simulate blade deformation during the diffusion bonding, hot twisting, hot stamping and gas bulging in sequence. After each forming step, the blade outer surface profile extracted from the simulation results can be compared with the experimental measurements to evaluate the FE model quality.

FE model setup

The diffusion bonding FE model is applied to simulate the blade deformation under the gravity load and expansion
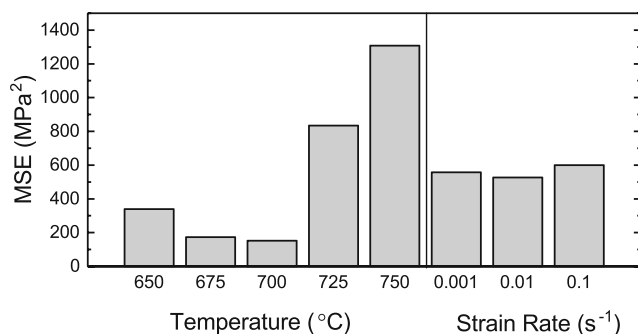
Fig. 14 MSEs of the hyperbolic-sine law model at different temperatures and strain rates

effects during the heating process. In the DB process, the two blade halves are assembled in the DB dies as shown in Fig. 15a and b. In the DB FE model, the blade halves can be regarded as one part and the additional positioning structures which has no influence on the blade deformation can be removed. As illustrated by Fig. 15c, the blade root is totally restricted in the DB tools and the gravity load is added to the blade. Y direction movement of the outer surface is also restricted by the inner surfaces of the DB tools as shown in Fig. 15d. The temperature field is added to the blade according to the recorded actual heating curve as given by Fig. 16. The difference between the programed heating path and the heating history recorded by a temperature recorder was caused by the insufficient heating power and heat transfer efficiency. In the simulations, the whole part was assumed being heated uniformly. Thermal expansion effects on the high temperature steel tools and TC4 blade can be simulated by defining the linear thermal expansion coefficient (CTE). The averaged CTE of TC4 during the temperature range of 100–900 °C is 8.9×10^{-9} °C^{-1} [23] while the expanded tool inner surfaces are applied taking the CTE of 13.6×10^{-9} °C^{-1} which is the averaged value at 700 °C provided by Xie et al. [24]. And the calibrated strain hardening form power law creep model is defined in the material model with temperature dependent coefficients.

In the FE modelling of the hot twisting, stamping and gas bulging processes, the calibrated hyperbolic-sine law equation is employed to define the constitutive relation.

The diffusion bonded hollow blade model extracted from the DB simulation result is applied in the hot twisting process simulation. As shown in Fig. 17, the blade root is fixed in the lower fixture while the head end is held by the upper fixture which rotates around the marked axis. In the FE model given by Fig. 17b, the lower fixture is removed by applying a total movement constraint to the root instead. The upper fixture holds and twists the blade to the required rotation angle with a rotation speed of 0.367 °/s. The rotation angle is determined by the diffusion bonded flat blade and the required final blade shape as illustrated in Fig. 18. The two ends of the blade heads in both the DB model and the required model are extracted to draw two vertical midlines. The rotation axis is vertical to the XY plane and goes through the intersection point of the vertical midlines. Fig. 17b shows the rotation direction and the total rotation angle α is 22 °. The blade heating history of the twisting process is also given in Fig. 19 to define the temperature field during the hot twisitng.

The hot twisting process can provide a rough shape hollow blade allowing to it to be installed on the lower stamping tool as shown in Fig. 20a. Then the hot stamping and gas bulging are performed to obtain a precise shape blade with machining allowance. In the closed stamping
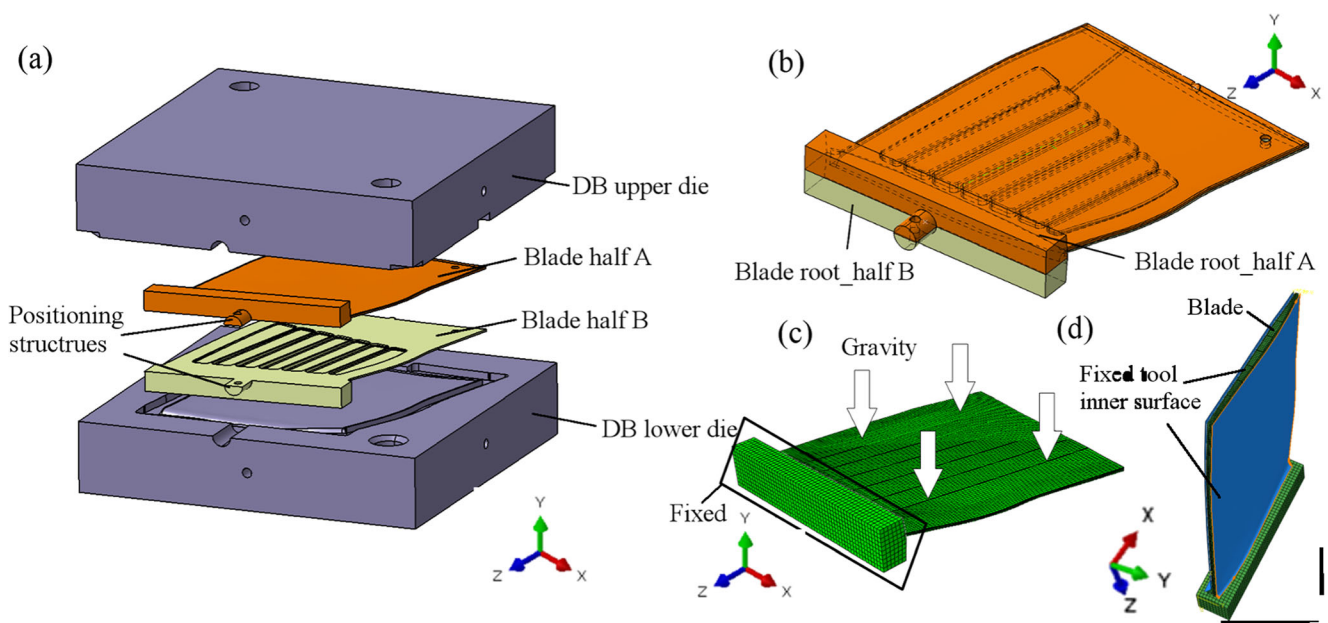
Fig. 15 The hollow blade DB model: **a** blade halves and DB tools; **b** assembled blade; **c** gravity load and blade root boundary condition in FE model; **d** boundary conditions of DB tool inner surfaces in FE model

tools as shown in Fig. 20b, the blade outer surface is bulged to the stamping tool inner surface by argon gas. The FE model is given in Fig. 20c. The stamping tool inner surfaces are used to stamp the blade and restrict its outer surface deformation during gas bulging. The blade root and the upper tool are fixed at the directions of X and Z while the lower tool movement is totally restricted. In the stamping process, the upper stamping tool moves along -Y direction at 0.05 mm/s and the total travel distance is 60 mm. In gas bulging, the gas pressure is added to the blade cavity inner surfaces. The heating history and gas

pressure load curve are given by Figs. 21 and 22 respectively.

Simulation results

The diffusion bonded hollow blade and the simulation result of the displacement distribution along Y direction are given in Fig. 23. The sinking depths of seven marked locations on the cavity surface at the cross section 125 mm away from the blade root bottom surface were measured. The measurement method is as shown in Fig. 24. A straight line is drawn with the two top points on the outer surface which are 1 mm away to the cavity walls. As the reinforcing rib height is consistent in the diffusion bonding process, the dash line shown in Fig. 24 is regarded as a reference to evaluate the outer surface sinking depth. The sinking depth D is determined as the distance between the lowest point on the outer surface and the dash line. The depth can be calculated with the marked points coordinates by following equation:

$$D = |[(Y2-Y1)X0 + (X1-X2)Y0 + Y1(X2-X1) \tag{7}$$

$$-X1(Y2-Y1)]/\sqrt{(Y2-Y1)^2 + (X2-X1)^2}|$$

where D is the sinking depth, $X0$ and $Y0$ are the selected sinking surface point coordinates, $X1$, $X2$, $Y1$ and $Y2$ are the coordinates of the surface points 1 mm from the cavity walls.

The calculated sinking depths are compared with the experimental measurements in Fig. 25. In the hot stamping simulation works [25], predictions of thickness with error less than 0.1 mm were considered precise in which both sides of
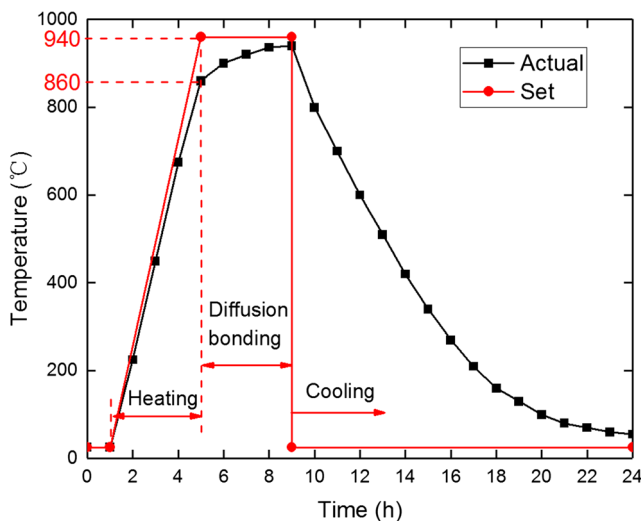
**Fig. 16** Heating history in diffusion bonding
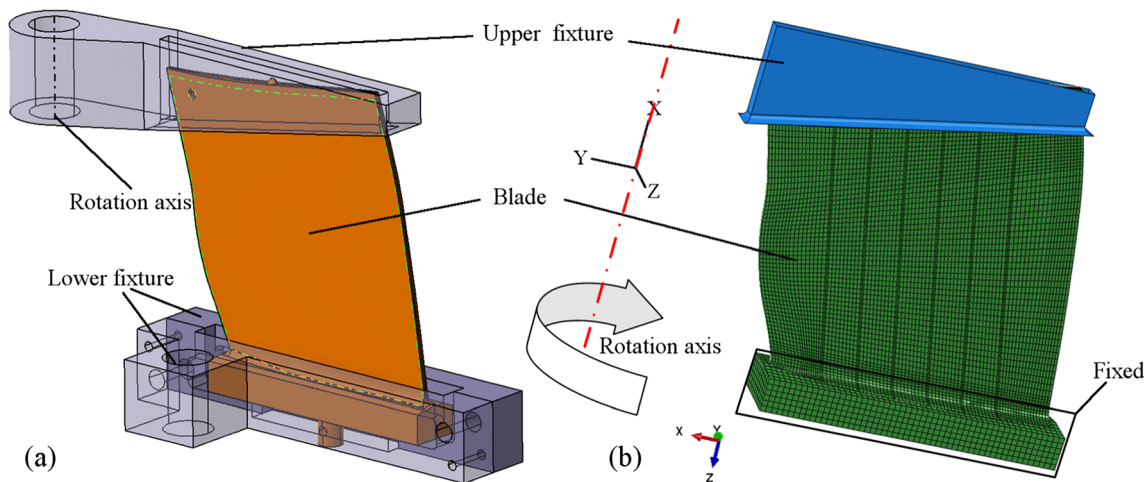
Fig. 17 Hollow blade hot twisting model: **a** blade and twisting fixtures; **b** blade root and upper twisting fixture rotation boundary conditions in FE model

the blank deformation was well restricted by the forming tools. For the simulation of the blade defects, the sinkage depth prediction error less than 0.2 mm are acceptable as the blade surface was not supported by any forming tools in this study. Both experiment measurement and simulation calculation show that the sinking is more serious at location of #1 and #7. The simulated sinking depths at most locations are higher than the measured depths. And at the grooves ends as indicated by the red circle in Fig. 23b, the surface sinkage is more

serious which are not predicted by the simulation. It is because the gas pressure produced by the air sealed between the upper diffusion bonding tool and the blade upper surface while the cavities are vacuumed which is connected the vacuum furnace through the air channel as marked in Fig. 1. For the discrepancies between the predictions and experimental measurements were caused by the constitutive relation and temperature field definitions. The sinkage depth were overestimated as the temperature field was uniformly added to the whole part

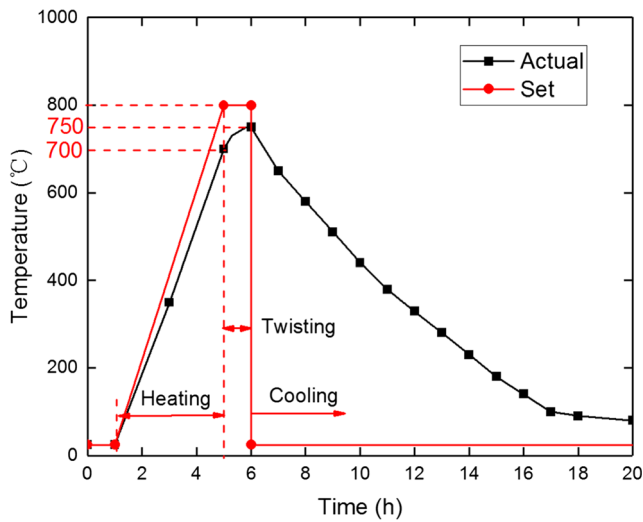**Fig. 18** Hollow blade hot twisting angle calculation
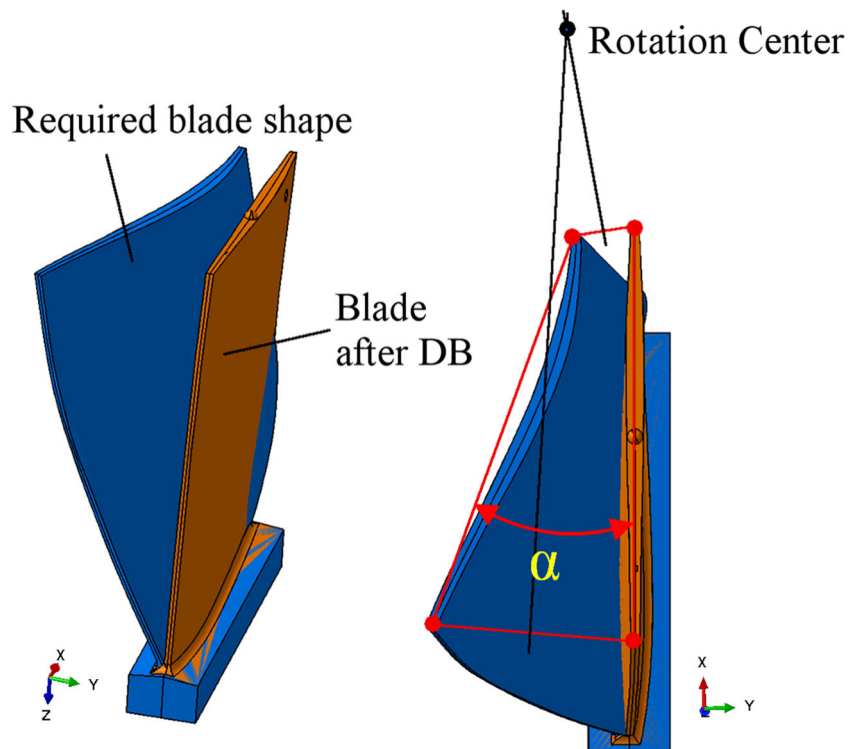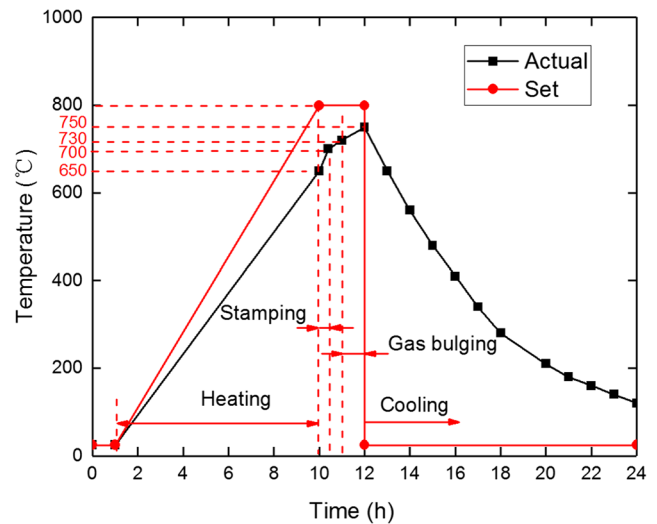
Fig. 19 Heating history in hot twisting

Fig. 21 Heating history in hot stamping and gas bulging process

applying the recorded temperature-time curve with thermal couple attached to the DB molds. The actual temperature of the blade should be lower than the curve given in Fig. 21.

The twisted blade is shown in Fig. 26. The section profile which is 125 mm from the blade root bottom plane is given by Fig. 27. The sinking depths of the marked locations are calculated with the same method mentioned above and compared with the measurements as shown in Fig. 28. The simulation overestimated the deformation during the twisting process. Compared the blade shape after twisting and diffusion bonding, it can be seen that the sinkage is more serious due to the twisting torque. And as indicated by the red circle in Fig. 26, the stress concentration area close to the blade root showed more serious sinkage. As the softening behavior was not simulated, the prediction for the twisting process was not so good

compared with the DB simulation results as shown in Figs. 25 and 28.

The simulated blade shape after hot stamping is given by Fig. 29a which shows more surface sinkage at the cavity locations. By comparing the blade shapes in Fig. 29b, c and d, it shows that the gas bulging process can effectively repair the surface to the required shape in both simulation and experiment. In Fig. 30, the predicted profile of the section 125 mm from the root bottom plane is compared with the required shape and actual blade part measurement. It also indicates that the blade outer surface defects produced in the diffusion bonding, twisting and stamping process can be well repaired. And the FE simulation accurately predicted the blade deformation after gas bulging.
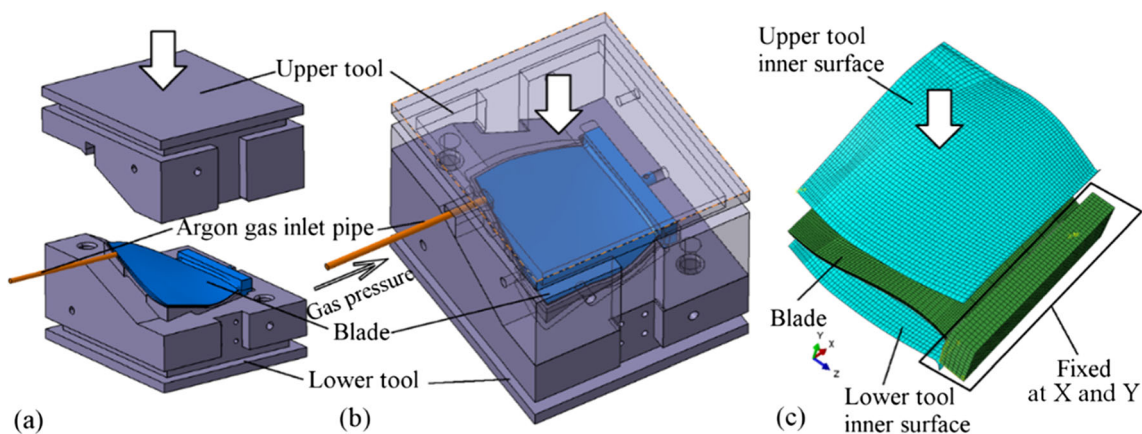

Fig. 20 Hollow blade hot stamping and gas bulging model: **a** blade installed on lower stamping tool; **b** blade in closed stamping tools; **c** blade root and upper stamping tool boundary condition
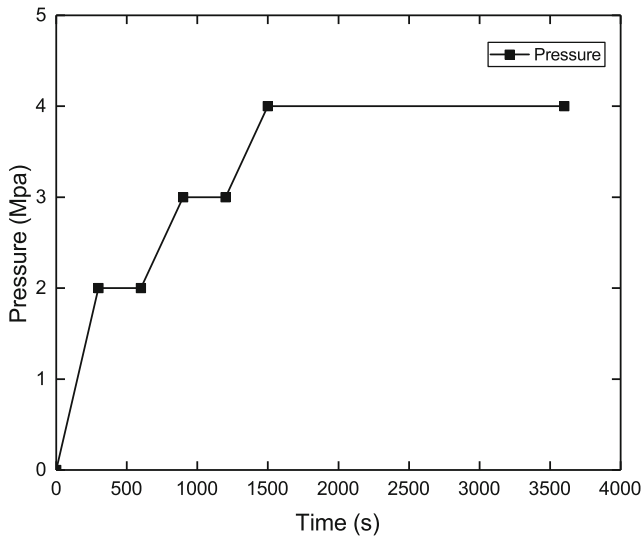
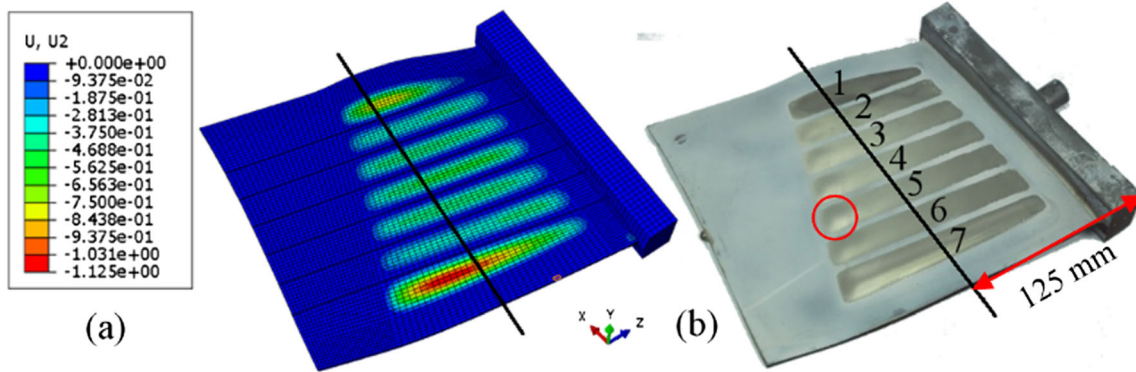**Fig. 22** Gas pressure load curve

Fig. 23 Diffusion bonded blade: **a** simulation result of the Y direction displacement (in mm); **b** experimental part

Conclusions

The TC4 hot flow behavior at the diffusion bonding and superplastic forming conditions were separately

characterized by carrying out isothermal hot tensile tests. A strain hardening form power law equation and a hyperbolic-sine law equation provided by the FE software Abaqus have been calibrated to describe the flow behavior

Fig. 24 Surface sinking depth measurement of the diffusion bonded blade at the section 125 mm from the blade bottom
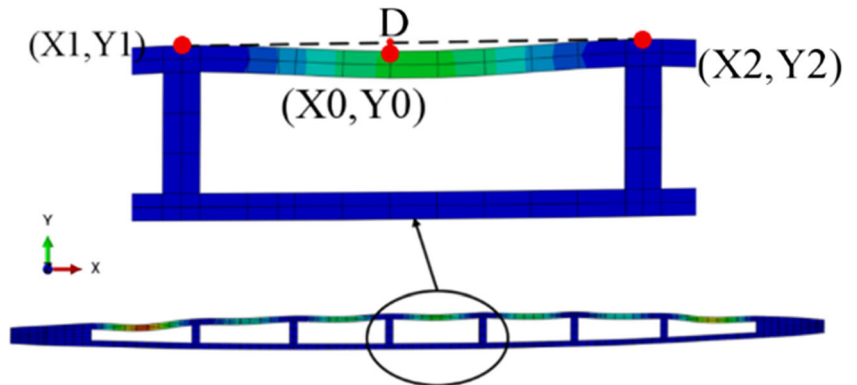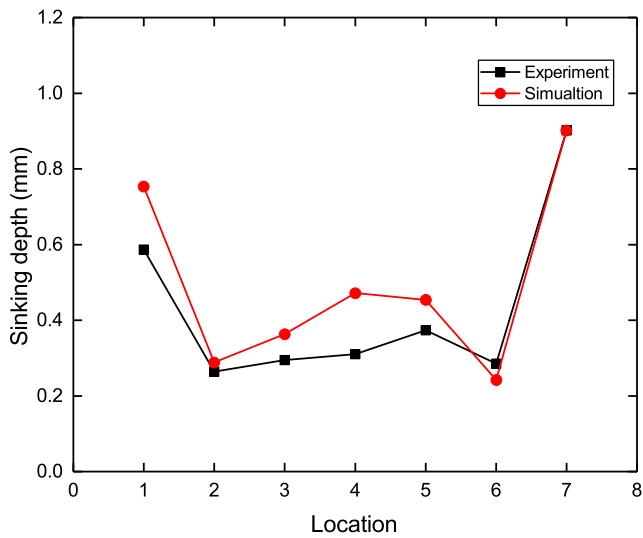
Fig. 25 Sinking depths after diffusion bonding of simulation and experiment

Fig. 26 Twisted blade: **a** simulation result of the Mises stress (in MPa); **b** experimental part
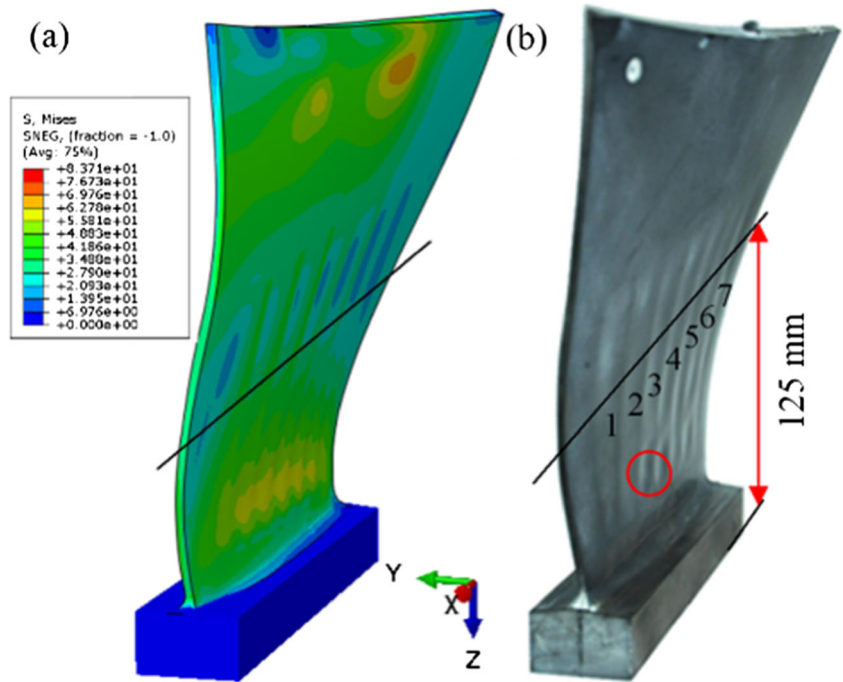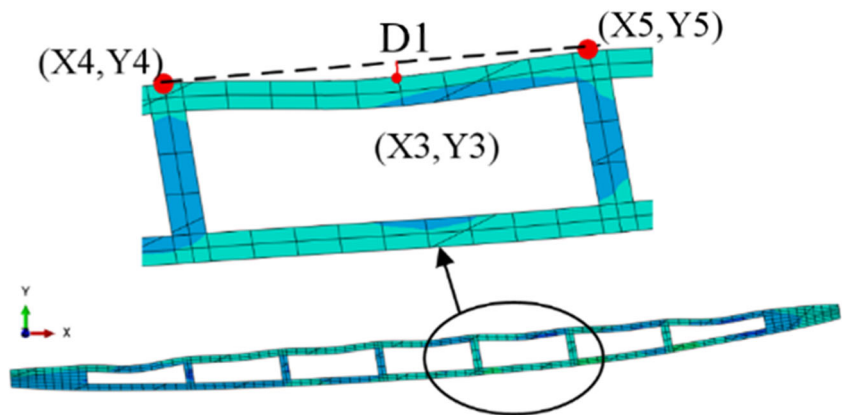

Fig. 27 Surface sinking depth measurement of the twisted blade at the section 125 mm from the blade bottom
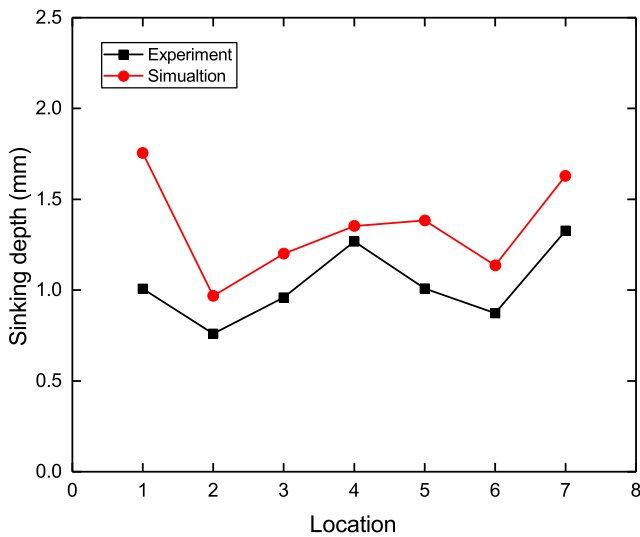
Fig. 28 Sinking depths after twisting of simulation and experiment

in the DB and SPF FE models respectively. According to the TC4 constitutive relation study and the FEA results, it can be concluded that:

1) In the DB temperature range of 860–940 °C and strain rate range of the 1×10^{-4} s^{-1} to 7×10^{-4} s^{-1}, the TC4 flow stress increased with strain during the uniaxial tensile test. Meanwhile the flow curves in the SPF temperature of 650–750 °C and strain rate range of the 10^{-3} s^{-1} to 10^{-1} s^{-1} showed obvious peak flow stress with continuous softening behavior caused by dynamic recrystallization and recovery. The DB creep model showed minor strain rate sensitivity in the small strain rate range applied in this study. The maximum strain in the DB simulation was 0.08425 of which the step time was 2 h. Tensile tests at strain rates ranging from 10^{-6} s^{-1} to 10^{-4} s^{-1} should be performed in future works to improve the DB process simulation accuracy.

2) The strain hardening form power law and hyperbolic-sine law creep model can accurately predict the DB flow curves and the peak stresses of the SPF flow curves respectively. And the equation parameters of both models are temperature and strain rate dependent.

3) The FE models with the calibrated constitutive equations are capable to predict the hollow blade surface defects during the SPF/DB process and forecast the outer surface sinkage. The gas pressure load curve is verified able to repair the hollow blade surface sinkage defects and assure meeting the shape requirement of the outer surface. The feasibility of the constitutive models and the FE models for TC4 hot flow behavior prediction in the hollow blade SPF/DB forming process are demonstrated.

4) In general, the simulations over predicted the sinkage defects for both the DB and hot twisting processes. To improve the simulation accuracy, more precise constitutive models considering the softening flow behavior and the strain path effects need to be established in future works. And thermal models for temperature field simulation are also very necessary to increase the model precision.
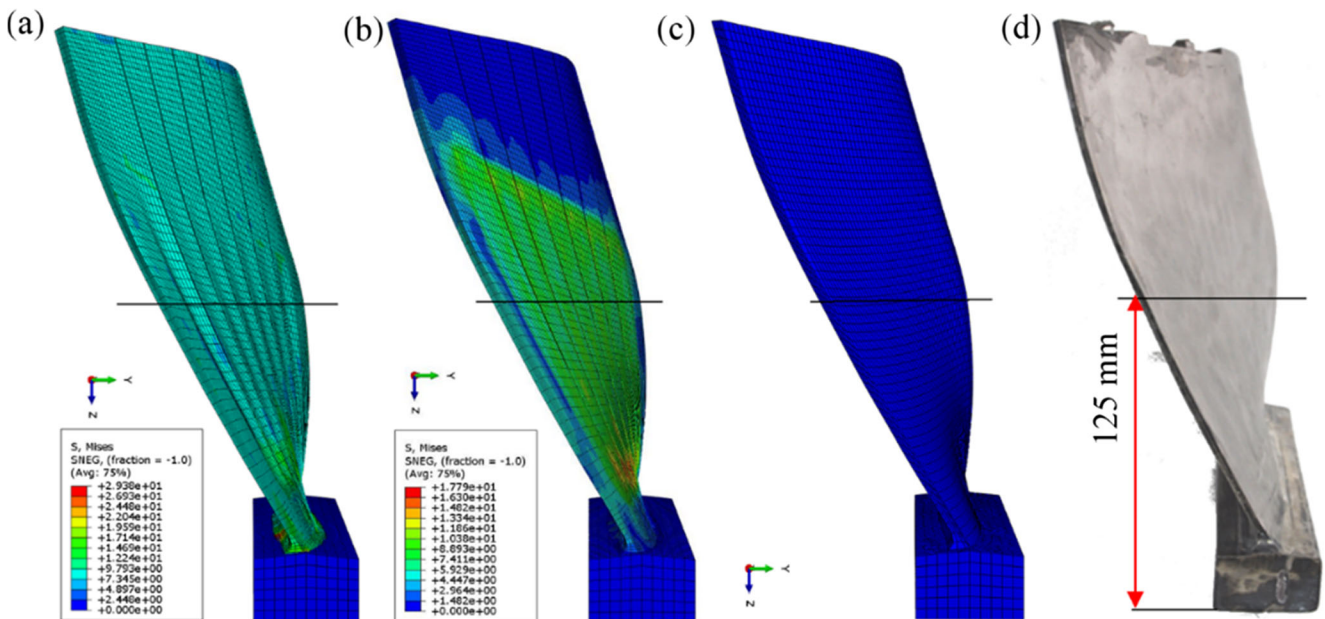

Fig. 29 Blade after hot stamping and gas bulging: **a** simulation result of Mises stress distribution after hot stamping (in MPa); **b** simulation result of Mises stress distribution after gas bulging (in MPa); **c** required blade shape; **d** blade after hot stamping and gas bulging

Fig. 30 Profiles of the blade section 125 mm from the blade bottom: **a** hot stamping simulation result and required blade shape; **b** gas bulging simulation result and experimental measurement; **c** gas bulging simulation result and required blade shape (in mm)
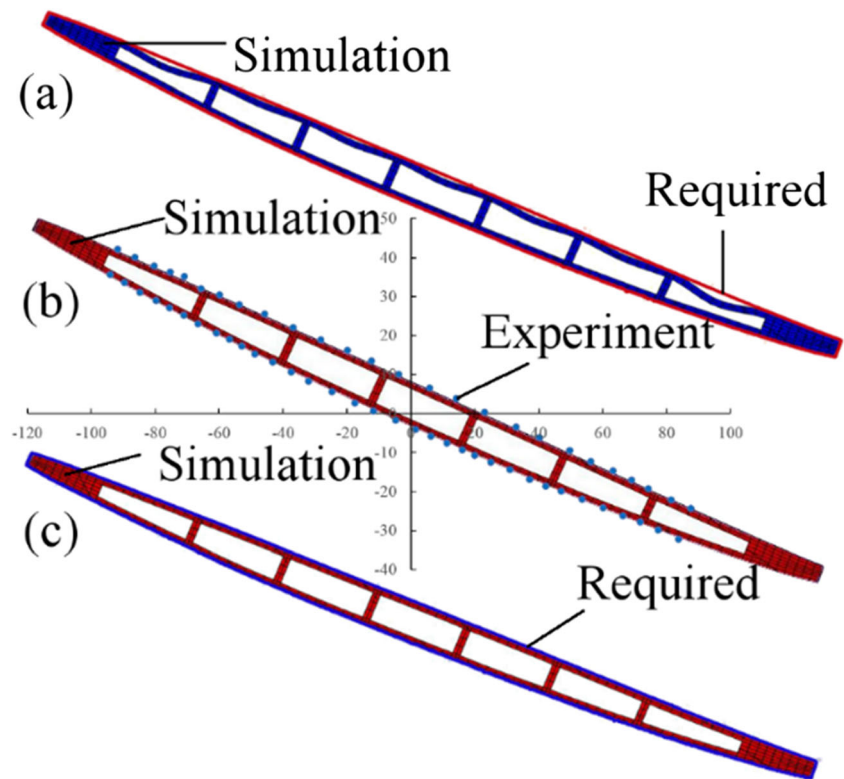
Compliance with ethical standards

Conflict of interest The authors declared that they have no conflicts of interest to this work.

Publisher's Note Springer Nature remains neutral with regard to jurisdictional claims in published maps and institutional affiliations.

References

1. Porter D, Dillner JR, Leibfried PE, Reimels WR, Asfalg GJ (1991) Method of forming a hollow blade. US Patent No. 5063662. U.S. Patent and Trademark Office, Washington, DC

2. Xun YW, Tan MJ (2000) Applications of superplastic forming and diffusion bonding to hollow engine blades. J Mater Process Technol 99(1-3):80–85. https://doi.org/10.1016/S0924-0136(99)00377-5

3. Zh Z, Xu J, Fu Y, Li Z (2017) An investigation on adaptively machining the leading and tailing edges of an SPF/DB titanium hollow blade using free-form deformation. Chin J Aeronaut 31(1):178–186. https://doi.org/10.1016/j.cja.2017.03.011

4. Ermachenko AG, Lutfullin RY, Mulyukov RR (2011) Advanced technologies of processing titanium alloys and their applications in industry. Rev Adv Mater Sci 29:68–821

5. Mavromihales M, Mason J, Weston W (2003) A case of reverse engineering for the manufacture of wide chord fan blades (WCFB) used in rolls Royce aero engines. J Mater Process Technol 134(3):279–286. https://doi.org/10.1016/S0924-0136(02)01108-1

6. Bichon M, Douguet CJP, Lorieux AGH, Louesdon YMJ, Renou, FAN (1997) Process for manufacturing a hollow blade for a turbomachine. US Patent No. 5636440. U.S. Patent and Trademark Office, Washington, DC

7. Bing Z, Zhiqiang L, Hongliang H, Jinhua L, Bingzhe B (2010) Three dimensional FEM simulation of titanium hollow blade forming process. Rare Metal Mater Eng 39(6):963–968. https://doi.org/10.1016/S1875-5372(10)60106-3

8. Sun S, Zong Y, Shan D, Guo B (2010) Hot deformation behavior and microstructure evolution of TC4 titanium alloy. Trans Nonferrous Metals Soc China 20(11):2181–2184. https://doi.org/10.1016/S1003-6326(09)60439-8

9. Momeni A, Abbasi SM (2010) Effect of hot working on flow behavior of Ti-6Al-4V alloy in single phase and two phase regions. Mater Des 31(8):3599–3604. https://doi.org/10.1016/j.matdes.2010.01.060

10. Shafaat MA, Omidvar H, Fallah B (2011) Prediction of hot compression flow curves of Ti-6Al-4V alloy in $\alpha+\beta$ phase region. Mater Des 32(10):4689–4695. https://doi.org/10.1016/j.matdes.2011.06.048

11. Bai Q, Lin J, Dean TA, Balint DS, Gao T, Zhang Z (2013) Modelling of dominant softening mechanisms for Ti-6Al-4V in steady state hot forming conditions. Mater Sci Eng A 559:352–358. https://doi.org/10.1016/j.msea.2012.08.110

12. Zhang T, Liu Y, Sanders DG, Liu B, Zhang W, Zhou C (2014) Development of fine-grain size titanium 6Al-4V alloy sheet material for low temperature superplastic forming. Mater Sci Eng A 608:265–272. https://doi.org/10.1016/j.msea.2014.04.098

13. Quan GZ, Luo GC, Liang JT, Wu DS, Mao A, Liu Q (2015) Modelling for the dynamic recrystallization evolution of Ti-6Al-4V alloy in two-phase temperature range and a wide strain rate

range. Comput Mater Sci 97:136–147. https://doi.org/10.1016/j.commatsci.2014.10.009

14. Quan GZ, Pan J, hua ZZ (2016) Phase transformation and recrystallization kinetics in space-time domain during isothermal compressions for Ti-6Al-4V analyzed by multi-field and multi-scale coupling FEM. Mater Des 94:523–535. https://doi.org/10.1016/j.matdes.2016.01.068

15. Tao ZJ, Yang H, Li H, Ma J, Gao PF (2016) Constitutive modeling of compression behavior of TC4 tube based on modified Arrhenius and artificial neural network models. Rare Metals 35(2):162–171. https://doi.org/10.1007/s12598-015-0620-4

16. Velay V, Matsumoto H, Vidal V, Chiba A (2016) Behavior modeling and microstructural evolutions of Ti-6Al-4V alloy under hot forming conditions. Int J Mech Sci 108–109:1–13. https://doi.org/10.1016/j.ijmecsci.2016.01.024

17. Luo J, Ye P, Li MQ, Liu LY (2015) Effect of the alpha grain size on the deformation behavior during isothermal compression of Ti-6Al-4V alloy. Mater Des 88:32–40. https://doi.org/10.1016/j.matdes.2015.08.130

18. Wu XC, Chen MH, Xie LS, Zhang TL, Hu ZH (2015) Twist-bend forming of aeroengine titanium tc4 wide-chord hollow fan blade with complex geometries. Acta Aeronaut Astronaut Sin 36(6): 2055–2063 (In Chinese)

19. Wu XC, Chen MH, Xie LS, Zhang TL, Hu ZH (2016) Creep repair of skin defects for the titanium TC4 wide-chord hollow fan blade. Rare Metal Mater Eng 45(11):190–195 (In Chinese)

20. Davenport SB, Higginson RL, Sellars CM et al (1999) The effect of strain path on material behaviour during hot rolling of FCC metals. Mater Design 66:1645–1661. https://doi.org/10.1016/j.matdes.2014.05.045

21. Tuninetti V, Gilles G, Milis O, Pardoen T, Habraken AM (2015) Anisotropy and tension-compression asymmetry modeling of the room temperature plastic response of Ti-6Al-4V. Int J Plast 67:53–68. https://doi.org/10.1016/j.ijplas.2014.10.003

22. Matsumoto H, Velay V, Chiba A (2015) Flow behavior and microstructure in Ti-6Al-4V alloy with an ultrafine-grained α-single phase microstructure during low-temperature-high-strain-rate superplasticity. Mater Des 66:611–617. https://doi.org/10.1016/j.matdes.2014.05.045

23. Jiang SS, Zhang KF (2009) Superplastic forming of Ti6Al4V alloy using ZrO2-TiO2 ceramic die with adjustable linear thermal expansion coefficient. Philos T Roy Soc A 357:1645–1661

24. Xie HJ, Wu XC, Min YA (2008) Influence of chemical composition on phase transformation temperature and thermal expansion coefficient of hot work die steel. J Iron Steel Res Int 15(6):56–61

25. Ilinich A, Luckey SG (2014) On Modeling the Hot Stamping of High Strength Aluminum Sheet. SAE Technical Paper 2014-01-0983. https://doi.org/10.4271/2014-01-0983